Theor Chem Acc (2011) 130:175–185
DOI 10.1007/s00214-011-0950-8

REGULAR ARTICLE

Theoretical study of the excited states and the redox potentials of unusually distorted β-trifluoromethylporphycene

Jun-ya Hasegawa · Kenji Matsuda

Received: 22 February 2011 / Accepted: 20 April 2011 / Published online: 11 May 2011
© Springer-Verlag 2011

Abstract Quantum chemical calculations were performed to analyze the excited states and the redox potentials of a recently synthesised fluorine-containing porphycene, 2,7,12,17-tetraethyl-3,6,13,16-tetrakis(trifluoromethyl) porphycene. The reduction and oxidation potentials of the porphycenes measured by cyclic voltammetry were semi-quantitatively reproduced using density-functional theory (DFT) and polarizable continuum model calculations, in which solvent effect and basis-sets extension effect were indispensable. Symmetry-adapted cluster configuration interaction and time-dependent (TD) DFT calculations were performed to analyze the visible region of the absorption spectra, and the results were in good agreement with the experimental data. The results of the calculations showed that both structural distortion and electronic effects cause specifically large stabilization of the LUMO level and become the origin of the particularly large positive-side shift of the reduction potential and the red-shift in the Q band absorption.

Dedicated to Professor Shigeru Nagase on the occasion of his 65th birthday and published as part of the Nagase Festschrift Issue.

Electronic supplementary material The online version of this article (doi:10.1007/s00214-011-0950-8) contains supplementary material, which is available to authorized users.

J. Hasegawa (✉) · K. Matsuda
Department of Synthetic Chemistry and Biological Chemistry, Graduate School of Engineering, Kyoto University, Kyoto-Daigaku-Katsura, Nishikyo-ku, Kyoto 615-8510, Japan
e-mail: hasegawa@sbchem.kyoto-u.ac.jp

J. Hasegawa
Quantum Chemistry Research Institute (QCRI) and JST-CREST, Kyodai Katsura Venture Plaza, North Building, 1-36 Goryo Oohara, Nishikyo-ku, Kyoto 615-8245, Japan

Keywords β-trifluoromethylporphycene · Excited states · Redox potentials · SAC-CI · TD-DFT

1 Introduction

Porphyrins are involved in a wide variety of redox reactions in proteins and bioinorganic metal complexes (for example see [1, 2]). Regulation of the redox potential of porphyrins [3] is one of the important aspects to functionalize the porphyrin-including systems. An interesting approach would be to introduce highly electron withdrawing, yet chemically inert peripheral substituents, such as a trifluoromethyl (CF_3) group [4, 5]. Another approach is to modify the structure of the tetrapyrrolic macrocycle. Porphycene [6] shown in Fig. 1 is one of the porphyrin isomers, and the positions of the pyrrole and methylene groups are interchanged. In particular, the reduction potential of porphycenes is more positive than that of porphyrin [3] because the LUMO level of porphycenes becomes more stable. The spatial symmetry of the porphycene macrocycle is C_{2h} symmetry and is lower than that of the porphyrin macrocycle (D_{4h} symmetry). Therefore, the breakdown of the degeneracy due to the symmetry lowering causes the stabilization of the LUMO level in porphycenes [7, 8].

Porphyrins and related compounds are also indispensable dyes and pigments. There are significant accumulations of studies concerning photoabsorption in visible regions. There are several strategies to modulate the Q band absorption. Substitution by heteroatoms in the macrocycle increases oscillator strength such as in azaporphyrins [9–11]. Introducing orbital interactions such as in phthalocyanine [12, 13] also increases the oscillator strength, and the peak position moves to lower energy

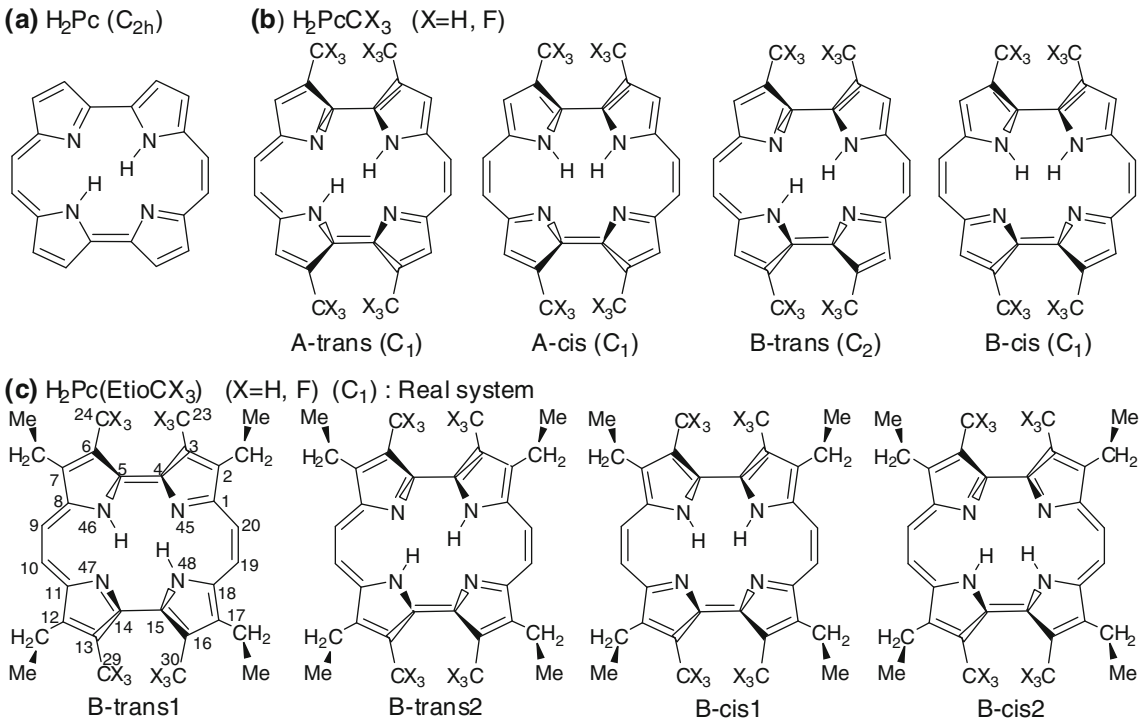

Fig. 1 Structures of the free-base porphycene compounds investigated in the present study. Molecular structural symmetry used for the calculations is indicated in the *parentheses*

region. The symmetry lowering of the macrocycle such as in chlorophylls and bacteriochlorophylls [14, 15] also increases absorption intensity of the Q band. The porphycene macrocycle also belongs to this class of compounds and has a Q band absorption larger than porphyrins [16, 17]. A combination of these strategies could produce excellent functional molecules such as phthalocyanine in which the strong absorption in the visible region is realized by the heteroatom substitutions and the introduction of orbital interactions [13].

Recently, the first fluorine-containing porphycene, 2,7,12,17-tetraethyl-3,6,13,16-tetrakis(trifluoromethyl) porphycene ($H_2Pc(EtioCF_3)$) was synthesised by Hayashi and coworkers [18]. Because of the electron-withdrawing nature of the CF_3 groups, the reduction and oxidation potentials shifted to the positive side. Another point of interest is a remarkable red-shift of the Q band by 0.17 eV. In the case of a fluorine-containing porphyrin, the amount of the red-shift was only 0.04 eV [5]. Suggested origins were the structural distortion effect introduced by the repulsion between the CF_3 groups [18]. Another possibility pointed out was the electronic interaction effect that arises from the electron-withdrawing nature of the CF_3 groups [18]. Clarifying the red-shift mechanism is an interesting subject because the CF_3 substitutions in H_2Pc might be a new strategy for controlling the Q band absorption.

In our previous studies, we analyzed the excited states of free-base porphin [19, 20], Mg porphin [21], chlorophylls [15], azaporphyrins [10, 11, 13], porphycene [17], hemiporphycene [17], and corphycene [17] to analyze the electronic structures and transition energies of the excited states. In the series of the studies, we are trying to systematically understand the strategies to control the Q band absorptions and emissions. We used the SAC [22]/SAC-CI [23–25] method [26, 27] that is a correlated method for calculating the excited states. Recently, a "direct algorithm" was implemented [28] in a recent version of the Gaussian package [29], in which the energy and the σ-vectors were computed directly from molecular integrals.

The present paper is aimed for analyzing the excited states and the redox potentials of the fluorine-containing porphycene. We also aimed for establishing a computational scheme to calculate the redox potentials and the excited states of porphyrin-related compounds. Reliable computations of these molecular properties would be very useful to understand the redox functions of molecules in environments and also to design photosensitizers for photovoltaic cells and photodynamic therapy. The present paper is organized as follows. In the next section, we mention the computational procedures employed in the present study. In Sect. 3, the energy levels of the frontier orbitals, so called the four orbitals, were discussed. Particularly, we investigated in a stepwise way how the

CF_3 substitutions change the orbital levels. In Subsection 3.2, we describe the results of quantum chemical calculations of the reduction and oxidation potentials. In Subsection 3.3, on the basis of the SAC-CI and DFT results, the origin of the red-shift is clarified in terms of the distortion and electronic effects.

2 Computational details

Figure 1 shows the porphycene compounds investigated in the present study. $H_2Pc(EtioCX_3)$ (X = H, F) shown in Fig. 1c corresponds to the real molecules synthesised in the experimental study [18]. In a X-ray crystallographic structural analysis [18], only a single conformation, B form, was observed (for definition, see Fig. 1 and latter description). H_2PcCX_3 (X = H, F) shown in Fig. 1b are simplified models in which the ethyl groups in $H_2Pc(EtioCX_3)$ were substituted by hydrogen atoms. We examined relative stability of two conformers, A and B forms, which represent different conformations of the four CX_3 groups. The positions of two hydrogen atoms within the four pyrrole rings were classified as "trans" and "cis" forms as shown in Fig. 1b, c. The symbol in the parentheses is molecular symmetry adopted in the calculations.

Regarding the basis sets, we use the following abbreviations. "Bas1" denotes the 6-31G* sets [30, 31] for all the atoms. "Bas2" is a combination of the 6-31G** [30, 31] sets for the H atoms at the $N_{pyrrole}$ atom and the 6-31G* sets for the other atoms. "Bas3" denotes the 6-311G** [32] sets for all the atoms.

Because the X-ray crystallographic structure is unusually distorted [18], it would be better to examine computational methods for optimizing the structures. It is also interesting that the present quantum chemical calculation can determine the protonation state of the pyrroles on the basis of the calculated structural parameters such as bond lengths, bond angles, and dihedral angles in addition to the relative energy difference. As we mentioned, the conformations of the CF_3 groups observed in the X-ray structure are the B form. In addition, all of the ethyl groups were in the same conformations as shown in Fig. 1c. The examined structures were, therefore, four patterns, B-trans1, B-trans2, B-cis1, and B-cis2. Computational model used was the $H_2Pc(EtioCF_3)$ model unless otherwise noted. The structural optimizations were performed without taking account of any environmental effect.

In Table 1, we compared relative energies, bond lengths, bond angles, and dihedral angles of $H_2Pc(EtioCF_3)$ in the different protonation states. More details of the comparison were described in Figure S1 in supplementary materials. On the basis of the results of the calculations, the B-trans2 form was concluded to be the best possible protonation state. The energy of the B-trans2 form was the lowest of all the isomers as shown in Table 1a. The cis forms were by 2–4 kcal/mol more unstable than the trans forms. Because the energy of the B-trans1 form is rather close to that of the B-trans2 form, we have to consider the results of the optimized structures. Table 1b shows the root mean square (rms) deviations and maximum deviations from the X-ray structure. For the bond length and bond angles, the rms and maximum deviations of the B-trans2 forms were the smallest of all the protonation states. On the other hand, the deviations of the dihedral angles, which are shown in Table 1b-3, slightly depended on the computational method and the DFT exchange–correlation functional. The maximum error occurs in the dihedral angles involving the CF_3 groups, for example C14–C15–C16–C30 (for the atom indices, see Fig. 1c). One reason is that the angles could depend on the interactions with the neighbor molecules in the actual crystal, which were not considered in the present calculations. Other reason is in the computational method. The B3LYP functional [33, 34] cannot describe dispersion interactions [35–37]. Concerning the MP2 result, the basis sets (the 6-31G* set for the F atoms) were insufficient for describing the dispersion effect. In contrast, the long-range corrected functional, CAM-B3LYP [38] and ωB97XD [39], gave the smallest deviation in the B-trans2 form. The ωB97XD functional also includes empirical dispersion term.

Next, we compare the results among the computational methods. Firstly, the dependence on the exchange–correlation functionals was small as seen in Table 1. Secondly, the basis-sets dependence is also small, indicating that even a B3LYP/6-31G* level calculation can give reliable structural parameters. Calculated relative energies in Table 1a also support this conclusion. Thirdly, we mention the effect of the simplification in the computational model from $H_2Pc(EtioCF_3)$ to H_2PcCF_3 (the ethyl group at the β positions were substituted to the H atoms). This simplification does not significantly affect the relative energies and structural parameters. The result for the bond lengths at the B3LYP/6-31G* level is shown in Table 1b, and the changes in the rms and maximum deviations were only 0.001 and 0.013 Å, respectively. In the case of the bond angles, the changes were 0.47° and 0.77°, respectively. In the case of the dihedral angles, the deviations became larger: 1.52° and 3.06°, respectively. Again, the largest deviation occurs at C14–C15–C16–C30 angle (8.64°), which involves the CF_3 group.

In calculating the reduction and oxidation potentials, we used electron affinity (EA) and ionization potential (IP), respectively. We performed computations for the real systems, $H_2Pc(EtioCH_3)$ and $H_2Pc(EtioCF_3)$ at the B3LYP/6-31G* level. With the Koopmans' theorem (KT), we used the LUMO and HOMO energies at the optimized structures

Table 1 Comparison of the energy and structural parameters of $H_2Pc(EtioCF_3)$

Computation[a]	B-trans1	B-trans2	B-cis1	B-cis2
(a) E_{rel} (kcal/mol)[b]				
B3LYP/Bas1	0.17	0.00	3.48	3.48
B3LYP/Bas3	0.13	0.00	3.21	3.21
CAM-B3LYP/Bas3	0.13	0.00	2.53	2.53
ωB97XD/Bas3	0.11	0.00	2.12	2.12
B3LYP/Bas1 (M)	0.00	0.00	3.80	3.80
MP2/Bas2 (M)	0.00	0.00	3.55	3.55
(b) RMS and Max deviations from the X-ray crystallographic structure[c]				
(b-1) Bond (Å)				
B3LYP/Bas1	0.017 (0.034)	0.009 (0.020)	0.017 (0.038)	0.018 (0.046)
B3LYP/Bas3	0.017 (0.033)	0.007 (0.017)	0.014 (0.035)	0.016 (0.038)
CAM-B3LYP/Bas3	0.018 (0.037)	0.010 (0.038)	0.022 (0.062)	0.024 (0.070)
ωB97XD/Bas3	0.016 (0.029)	0.006 (0.016)	0.022 (0.044)	0.024 (0.053)
B3LYP/Bas1 (M)	0.018 (0.038)	0.010 (0.033)	0.021 (0.067)	0.020 (0.058)
MP2/Bas2 (M)	0.022 (0.069)	0.019 (0.069)	0.026 (0.094)	0.025 (0.087)
(b-2) Angle (°)				
B3LYP/Bas1	2.36 (4.40)	0.54 (1.30)	1.63 (3.79)	1.42 (3.64)
B3LYP/Bas3	2.31 (4.43)	0.51 (1.29)	1.59 (3.83)	1.38 (3.61)
CAM-B3LYP/Bas3	2.30 (4.69)	0.51 (1.26)	1.62 (4.53)	1.38 (3.47)
ωB97XD/Bas3	2.30 (4.68)	0.53 (1.37)	1.65 (4.76)	1.40 (3.41)
B3LYP/Bas1 (M)	2.57 (5.28)	1.01 (2.07)	1.60 (3.67)	1.79 (4.48)
MP2/Bas2 (M)	2.54 (5.03)	0.85 (1.46)	1.67 (3.88)	1.80 (4.24)
(b-3) Dihedral (°)				
B3LYP/Bas1	3.02 (5.57)	2.52 (5.58)	2.78 (5.25)	2.37 (4.95)
B3LYP/Bas3	2.91 (5.37)	2.43 (4.92)	2.84 (4.71)	2.36 (5.37)
CAM-B3LYP/Bas3	3.21 (6.03)	2.68 (5.11)	3.82 (6.52)	3.01 (7.13)
ωB97XD/Bas3	3.43 (6.34)	2.62 (4.87)	4.46 (7.46)	3.55 (8.59)
B3LYP/Bas1 (M)	4.39 (7.31)	4.04 (8.64)	3.30 (5.14)	3.62 (7.43)
MP2/Bas2 (M)	3.96 (6.92)	3.21 (6.31)	3.02 (5.16)	2.52 (5.58)

[a] Bas1: 6-31G*. Bas2: 6-31G** for the H atoms at the N atom of pyrrole rings, and 6-31G* for the other atoms. Bas3: 6-311G**. "(M)" denotes that four ethyl groups were substituted by the H atoms (the H_2PcCX_3 model). The B-trans1 and B-trans2 forms become identical when the ethyl groups were removed. The same is for the B-cis1 and B-cis2 models

[b] Relative energy compared with the total energy of the B-trans2 form

[c] Root mean square deviation. Number in the parenthesis is the maximum deviation

of the neutral species. In the next, adiabatic EA and IP were used for including electronic relaxation and molecular structural relaxation effects. Thermal effects were taken into account by using Gibbs free energy at 298.16 K. Zero-point energy, vibration, rotation, and translational energies were included in the internal energy. Finally, the basis-sets extension effect was taken into account in the adiabatic EA and IP. At the optimized structures for the reduced, neutral, and oxidized species, single-point calculations were performed at the B3LYP/6-311+G** level. The energy difference from the B3LYP/6-31G* result was added to the adiabatic EA and IP at the B3LYP/6-31G* level. We tried to include diffuse functions at the optimization step. However, SCF convergence became very bad when a PCM was combined. All of these calculations included the solvent effect in the electronic energies. Self-consistent reaction field method with a PCM [40] was adopted. Dielectric constant of PhCN was used to mimic the experimental condition [18].

A computational strategy to approach the experimental oxidation and reduction potentials was studied in previous articles [41, 42]. These previous studies used extrapolation corrections for the solvent effect, the thermal effect, and the basis-sets extension effects. However, the solvent effect determines the largest part of EA and IP. In addition, an empirical correction was also included to improve the B3LYP description of the IP [42]. In the present study, we already included the solvent effect in the structural optimizations and the frequency calculations. The single-point 6-311+G** calculations also included the solvent effect. To calculate the reduction and oxidation potentials with the Ag/AgCl reference electrode, we have to consider a half-reaction, $AgCl(s) + e^- \rightarrow Ag(s) + Cl^-(aq)$. The reduction potential of the half-reaction is −0.22 V (vs. normal hydrogen electrode (NHE) [43]). Therefore, we need to calculate reduction and oxidation potentials of the porphycenes when NHE is used. To calculate these potentials, we used a reaction Gibbs free energy $\Delta_r G$ of a

half-reaction, $H^+ + e^- \rightarrow (1/2)H_2(g)$, that was estimated to be −4.44 eV in a previous study [44]. Together with the quantum chemically calculated EA and IP, the reduction and oxidation potentials of the porphycenes with the NHE were calculated. In the last step, the potentials with the Ag/AgCl electrode were evaluated. Nernst equation [43] was used for the conversion between the potentials and Gibbs free energy.

Excited states of H_2Pc, H_2PcCH_3, H_2Pc_distorted, and H_2PcCF_3 were calculated with SAC-CI and TD-DFT [45, 46] with the B3LYP and LC [47]-BLYP [34, 48] functionals. To separate the distortion effect from the electronic effect in $H_2Pc(EtioCF_3)$, we introduced H_2Pc_distorted, a distorted H_2Pc model, in which atomic coordinates were taken from the fully optimized structure of H_2PcCF_3 except that the CF_3 groups were substituted by the hydrogen atoms.

For the TD-B3LYP and TD-LC-BLYP calculations, the 6-311G** basis sets were used. The ground-state molecular structures were optimized at the B3LYP/6-311G** and LC-BLYP/6-311G** levels for the TD-B3LYP and TD-LC-BLYP calculations, respectively. For the SAC-CI calculations, the LC-BLYP/6-311G** optimized structures were used. The D95(d) basis sets [49] were used. Analysis of the MO energy levels is very useful to understand the result of the excited-state calculations. We analyzed the Hartree–Fock (HF) MOs to understand the SAC-CI results.

Concerning the SAC-CI calculations performed in this study, we solved both variational (SAC-CI-V) and non-variational (SAC-CI-NV) equations [24] for the SAC-CI eigenvalue problem. The SAC-CI-V equation was derived as an approximation to the one exactly derived by the variational principle. The SAC-CI-NV equation was obtained by projecting Schrödinger equation on the configurations defined with the linked operators. See the original publications [23–25] for details.

All of the computations were performed with the Gaussian09 package [29].

3 Results and discussion

3.1 Effect of the CF_3 and CH_3 substitutions on the four orbital levels

Figure 2 shows Hartree–Fock MO distributions and energy levels of the four orbitals of the porphycene compounds, H_2Pc, H_2PcCH_3, H_2Pc_distorted, and H_2PcCF_3. There are two high-lying occupied (HOMO and next HOMO) and two low-lying unoccupied orbitals (LUMO and next LUMO) such as porphyrin compounds. These orbitals were relevant to the wave functions of the low-lying excited states as described in the latter section. In analogy to the porphyrin case [50], we use "four orbitals" for next HOMO, HOMO, LUMO, and next LUMO. In the case of D_{4h} symmetry as in metalloporphyrins, the LUMO and next LUMO levels are degenerate. In the C_{2h} symmetry case of porphycene, the LUMO and next LUMO levels were separated by 0.43 eV. On the other hand, the HOMO and next HOMO levels were close to each other.

Next, we investigate the effect of the CF_3 substitutions on the orbital energy levels. The previous report pointed out two effects [18]. The first one is structural distortion of the π skeleton induced by the steric repulsion of the CF_3 groups. To investigate the distortion effect, we introduced the H_2Pc_distorted model. The second one is electrostatic effect that arises from the electron-withdrawing property of the CF_3 groups. Comparing the orbital energy levels of H_2Pc and H_2Pc_distorted, the LUMO level of the distorted model showed specific low-energy shift of −0.12 eV, while the shift of the other MOs were relatively smaller as seen in Fig. 2. Because LUMO of H_2Pc has an antibonding

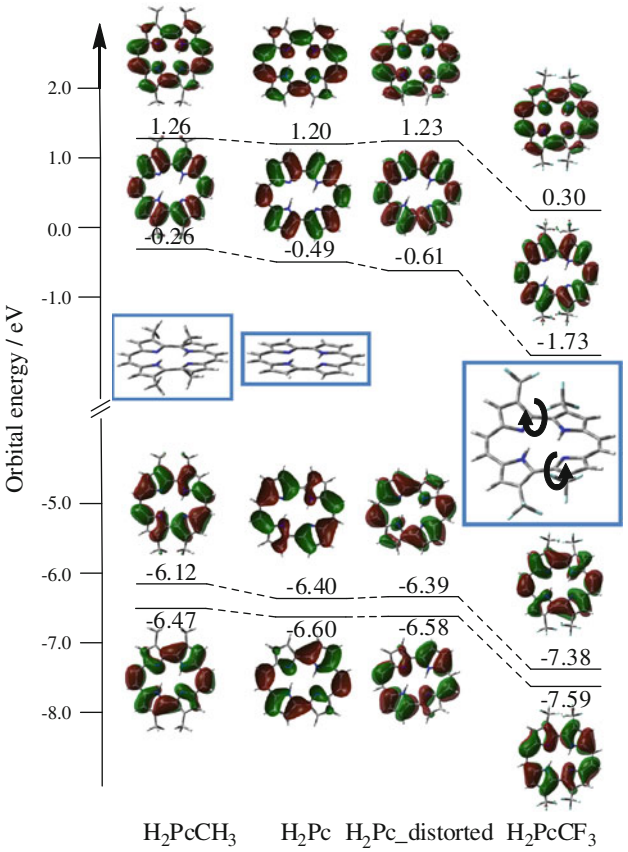

Fig. 2 Hartree–Fock MO distributions (isosurface value = 0.02) and orbital correlation diagram of the four orbitals of the porphycene compounds. The *number* next to the *bar* is the orbital levels in eV. Calculations were performed at the HF/D95(d)//LC-BLYP/6-311G** level. *Insets* show the optimized structures of H_2PcCH_3, H_2Pc, and H_2PcCF_3. For the H_2Pc_distorted model, the geometry of the porphycene skeleton is the same as that of H_2PcCF_3

interaction at the C4–C5 and C14–C15 bonds, the distortions introduced in the C4–C5 and C14–C15 bonds (see insets of Fig. 2) stabilize the LUMO level. Introducing the CF_3 groups in the H_2Pc_distorted model, all of the four orbitals showed significant low-energy shifts by −0.93 to −1.12 eV. In particular, the shift of the LUMO level (−1.12 eV) was the most significant. This specific shift would be ascribed to the LUMO distribution. As seen in Fig. 2, LUMO has larger distribution on the C3, C6, C13, and C16 moieties than the other four orbitals. Therefore, the largest electron-withdrawing effect of the CF_3 groups was observed in the LUMO level. We conclude that both the steric distortion and the electronic effects contribute specific low-energy shift of the LUMO level.

Introducing methyl groups at the C3, C6, C13, and C16 positions of H_2PcCH_3 also causes a red-shift of the Q band position as in the CF_3 case. However, the methyl substitution effect causes high-energy shifts in the HOMO and LUMO levels as shown in Fig. 2. The amount of the shift in HOMO and LUMO was 0.28 and 0.23 eV, respectively, which slightly reduced the HOMO–LUMO gap compared with that of H_2Pc. There are two effects that explain the reason. The first one is a hyper-conjugation between the methyl groups and the π skeleton of the porphycene ring: antibonding interactions between the C–H σ orbitals, and the π orbitals pushed up the HOMO and LUMO levels (See Figure S2 in supplementary material). The second one is the structural distortion effect as in the CF_3 case. Although the extent of the distortion is much smaller than that of H_2PcCF_3, the C3–C4–C5–C6 dihedral angle was calculated to be 9.8°. Because the distortion specifically stabilizes the LUMO levels, the HOMO–LUMO gap became smaller in H_2PcCH_3.

3.2 On the significant positive-side shift of the redox potentials

In order for computational chemistry to be a useful tool for designing a redox reagent, it is necessary to calculate the redox potentials of a molecule at least in a semiquantitative accuracy. We performed DFT calculations to reproduce the experimental reduction and oxidation potentials with the Ag/AgCl reference electrode. At first, we mention the accuracy of the KT level estimation using the HF/D95(d)//LC-BLYP/6-311G** results. As shown in Fig. 2, the CF_3 substitutions significantly reduced the orbital energies of the four orbitals, showing that at least the trend was reproduced. However, the KT level estimation for the reduction and oxidation potentials of H_2PcCF_3 was −2.71 and 2.72 V, respectively. These values were far from the experimental reduction (−0.14 V) and oxidation (+0.92 V), respectively. These errors cannot be improved if we calculate a real molecule, $H_2Pc(EtioCF_3)$, without any omission of the substituents (reduction: −3.01 V, oxidation: +2.28 V). Next, we used adiabatic EA and IP calculated at the B3LYP/6-31G*//B3LYP/6-31G* level. Calculated reduction and oxidation potentials of $H_2Pc(EtioCH_3)$ were −3.52 V and +1.33 V, respectively, which were still far from the experimental data (reduction: −0.92 V, oxidation: +0.92 V).

The first important improvement was achieved by including the solvent effect at the PCM level. The results were shown in Table 2. At the KT level, the calculated potentials were in a crude agreement with the experimental data. The largest error was around 0.9 V on the reduction potentials. With the use of the adiabatic EA and IP, the results for the calculated potentials were further improved by around 0.2 V. Including the thermal effect using Gibbs free energy (at 278.15 K), minor change at most 0.1 V was obtained. The second important improvement around 0.3–0.4 V was obtained by the basis-sets extension from the 6-31G* to 6-311+G** sets. The calculated reduction and oxidation potentials of $H_2Pc(EtioCF_3)$ were −0.35 V and +1.04 V, respectively, which were in qualitative agreement with the experimental data (−0.14 V and +1.30 V, respectively). For $H_2Pc(EtioCH_3)$, similar qualitative agreement was achieved. We also note that the relative differences were in very good agreement at the KT level. This substituent effect, the $\Delta(CF_3–CH_3)$ values, in the oxidation and reduction potentials were calculated to be +0.49 and +0.82 V, respectively (in experiment, +0.38 and +0.78 V, respectively).

In the experiment, a specifically large positive-side shift was observed in the reduction potential when the CF_3 groups were introduced [18]. Because the shift was almost reproduced at the KT level, the origin is ascribed to the specific stabilization of the LUMO level in PhCN solution as seen in the MO diagram (see Fig. 2).

The difference between the oxidation and reduction potentials is a good measure for the HOMO–LUMO gap. This quantity became gradually accurate as shown in Table 2. After all of the corrections were included, calculated gaps for $H_2Pc(EtioCF_3)$ and $H_2Pc(EtioCH_3)$ were +1.39 and +1.83 V, respectively. These numbers were in very good agreement with the experimental data for $H_2Pc(EtioCF_3)$ (+1.44 V) and $H_2Pc(EtioCH_3)$ (+1.84 V). We also note that the substituent effect, the $\Delta(CF_3–CH_3)$ value, was already in a quantitative accuracy at the KT level estimation.

We also performed MP2 calculations for the redox potential. Because the optimization at the MP2/6-31G* level was time-consuming, we performed single-point MP2/6-311+G(d,p) calculations with PCM at the B3LYP/6-31G* optimized geometry. For $H_2PcEtioCH_3$, the calculated reduction and oxidation potentials were −2.58 and 1.96 V, respectively. We found that the <S**2> value for the doublet anion and cation states were 1.17 and 1.14,

Table 2 Calculated and experimental oxidation and reduction potentials (V) of H_2PcCF_3 and H_2PcCF_3

	B3LYP/6-31G*	B3LYP/6-31G* + PCM				Exptl.[a]
	KT	KT	E_{el}	G	G + Δ^{basis}	
Oxidation						
$H_2Pc(EtioCF_3)$	+1.05	+1.01	+0.79	+0.73	+1.04	+1.30
$H_2Pc(EtioCH_3)$	+0.23	+0.52	+0.31	+0.29	+0.55	+0.92
$\Delta(CF_3–CH_3)$	+0.82	+0.49	+0.48	+0.44	+0.49	+0.38
Reduction						
$H_2Pc(EtioCF_3)$	−1.07	−1.07	−0.86	−0.76	−0.35	−0.14
$H_2Pc(EtioCH_3)$	−2.15	−1.89	−1.67	−1.59	−1.28	−0.92
$\Delta(CF_3–CH_3)$	+1.08	+0.82	+0.81	+0.83	+0.83	+0.78
Oxidation potential minus reduction potential						
$H_2Pc(EtioCF_3)$	+2.12	+2.08	+1.65	+1.49	+1.39	+1.44
$H_2Pc(EtioCH_3)$	+2.38	+2.41	+1.98	+1.88	+1.83	+1.84
$\Delta(CF_3–CH_3)$	−0.36	−0.33	−0.33	−0.39	−0.34	−0.40

"KT" denotes that the reduction and oxidation potentials were calculated with EAs and IPs at the Koopman theory level. "E_{el}" denotes that the potentials were calculated with adiabatic EAs and IPs. "G" denotes that Gibbs free energy was used. "G + Δ^{basis}" denotes that the basis-sets extension effect was included. "Δ^{basis}" is the energy difference between the 6-311+G** and the 6-31G* results. "$\Delta(CF_3–CH_3)$" denotes the difference between $H_2Pc(EtioCF_3)$ and $H_2Pc(EtioCH_3)$

[a] The first oxidation and reduction potentials. Experimental data measured using cyclic voltammetry in PhCN using the Ag/AgCl reference electrode. See Ref. [1]

respectively, which were far from the desirable value for a doublet state. We, therefore, performed the approximated spin projection proposed [51, 52] to improve the spin contamination. Although the reduction and oxidation potentials were improved by 0.30 and 0.15 V, respectively, the agreement to the experimental data is still worse than the B3LYP results. We note that B3LYP gave correct expectation values (0.757 and 0.762 for anion and cation states, respectively).

The messages obtained by the series of calculations were the crucial importance of the solvent effect. To discuss relative shift in the potentials, a KT level estimation using the orbital energies at neutral geometry was satisfactory. We note, however, the KT level estimation for the $\Delta(CF_3–CH_3)$ values fails when the solvent effect was not included as shown in Table 2. Extended basis sets were necessary to achieve semiquantitative agreement with the experimental data. For improving the quantum chemical calculations of the redox potentials in a future study, the description of the environmental effect would be a key point because the solvent effect shares an essential portion of the calculated potentials.

3.3 Low-lying excited states of H_2Pc, H_2Pc_distorted, H_2PcCF_3, and H_2PcCH_3

In Table 3, we summarized excited states calculated with the SAC-CI and TD-DFT methods. Calculated excitation energies were compared with that of the experimental data [18]. Excitation energies calculated with the SAC-CI-NV equations were in reasonable agreement with the experimental data. Regarding the first excitation energy, the deviations from the experimental data for H_2Pc, H_2PcCF_3, and H_2PcCH_3 were −0.07, −0.17, and −0.17 eV, respectively. The SAC-CI-V excitation energies were systematically smaller than those with the SAC-CI-NV ones. The deviations from the SAC-CI-NV results were −0.10, −0.07, −0.08, −0.06 eV for H_2Pc, H_2PcCH_3, H_2Pc_distorted, and H_2PcCF_3, respectively. Calculated oscillator strengths were very close to those obtained with the SAC-CI-NV solutions.

The excited-state wave functions are more or less similar among the porphycene compounds. In the case of H_2Pc, the first excited state, the 1^1B_u state, was dominated by next HOMO → LUMO transition (64% in weight). In the second excited state, the 2^1B_u state, was represented by the HOMO → LUMO transition (67% in weight). These leading configurations were unchanged after the CH_3 and CF_3 substitutions.

Here, we explain the origin of the red-shift of the Q band when the CF_3 groups were introduced in the H_2Pc. As described above, the CF_3 effects were analyzed in twofold: structural distortions and electronic interactions. As shown in Table 3, introducing the structural distortion in the H_2Pc_distorted model, the excitation energies for the first and second excited states were shifted to 1.64 and 1.94 eV, respectively, which were by 0.25 and 0.22 eV smaller than those of H_2Pc. In H_2PcCF_3, the first and

Table 3 Low-lying excited states of H_2Pc, H_2PcCH_3, H_2Pc_distorted, and H_2PcCF_3

State	SAC-CI-NV[a,b]		SAC-CI-V[a,b]	B3LYP[c]	LC-BLYP[d]	Exptl.
	$E_{ex}(f)$[e]	Main configurations (|C| ≥ 0.2)	$E_{ex}(f)$[e]	$E_{ex}(f)$[e]	$E_{ex}(f)$[e]	$E_{ex}(f)$[e]
(1) H_2Pc (C_{2h} symmetry), MO81 = HOMO, MO82 = LUMO						
1^1B_u	1.89 (0.17)	−0.81 (80 → 82) −0.44 (81 → 83)	1.79 (0.16)	2.22 (0.13)	1.95 (0.15)	1.96[f], 1.98 [g]
2^1B_u	2.16 (0.30)	−0.82 (81 → 82) +0.34 (80 → 83) +0.22 (80 → 82)	2.06 (0.31)	2.34 (0.20)	2.12 (0.23)	2.07[f]
(2) H_2PcCH_3 (C_2 symmetry), MO97 = HOMO, MO98 = LUMO						
1^1B	1.72 (0.14)	−0.75 (96 → 98) −0.41 (97 → 99) −0.32 (97 → 98)	1.65 (0.13)	2.19 (0.12)	1.90 (0.13)	1.89 [h,i]
2^1B	2.02 (0.30)	−0.78 (97 → 98) +0.36 (96 → 98) +0.30 (96 → 98) +0.22 (97 → 99)	1.95 (0.30)	2.32 (0.22)	2.09 (0.25)	
(3) H_2Pc_distorted (C_2 symmetry), MO81 = HOMO, MO82 = LUMO						
1^1B	1.64 (0.18)	+0.80 (80 → 82) −0.39 (81 → 83) +0.22 (81 → 82)	1.56 (0.17)	2.12 (0.14)	1.85 (0.17)	
2^1B	1.94 (0.31)	+0.85 (81 → 82) +0.33 (80 → 83) −0.19 (80 → 82)	1.86 (0.30)	2.26 (0.20)	2.06 (0.24)	
(4) H_2PcCF_3 (C_2 symmetry), MO145 = HOMO, MO146 = LUMO						
1^1B	1.55 (0.19)	−0.69 (144 → 146) +0.49 (145 → 146) −0.31 (145 → 147) −0.20 (144 → 147)	1.49 (0.19)	2.04 (0.16)	1.77 (0.13)	1.72
2^1B	1.89 (0.32)	+0.68 (145 → 146) +0.56 (144 → 146) −0.24 (144 → 147) +0.19(145 → 147)	1.80 (0.32)	2.20 (0.22)	2.00 (0.28)	

[a] "NV" and "V" denote that the solutions were obtained with the SAC-CI non-variational and variational equations, respectively

[b] SAC-CI/D95(d)//LC-BLYP/6-311G** calculations

[c] B3LYP/6-311G**//B3LYP/6-311G** calcuations

[d] LC-BLYP/6-311G**//LC-BLYP/6-311G** calcuations

[e] Excitation energy in eV. Number in parenthesis denotes oscillator strength in atomic unit

[f] In 2-methyltetrahydrofuran. Ref. [2]

[g] In benzene. Ref. [3]

[h] 2,7,12,17-tetraethyl-3,8,13,18-tetramethylporphycene in CH_2Cl_2 [1]

[i] 2,7,12,17-tetraethyl-3,8,13,18-tetramethylporphycene [4]

second excitation energies were further shifted to 1.55 and 1.89 eV, respectively, which were by 0.11 and 0.05 eV smaller than those of H_2Pc_distorted. The 74% of the shift arose from the distortion, while the rest of the 26% from the electronic effect. These results indicate that the major origin of the Q band shift is ascribed to the structural distortion introduced by the steric repulsion of the CF_3 groups. A key point to understand the results of the calculations is that the Q bands originate from the excitations to LUMO. As mentioned in the former section, both the structural and electronic effects contribute to the specific stabilization of the LUMO level.

Next, we mention the DFT results. The excitation energy with TD-B3LYP was by 0.26–0.32 eV higher than the experimental data, and the deviations were rather systematic among the porphycenes. On the other hand, very fine agreement was obtained with the long-range corrected (LC)-BLYP functional [47, 53]. The deviations from the experimental data for H_2Pc, H_2PcCH_3, and H_2PcCF_3 were −0.01, +0.01, and +0.05 eV, respectively. Oscillator strengths calculated with the B3LYP and LC-BLYP functions were in qualitative agreement with those obtained with the SAC-CI method. In Table S1, in supplementary material, we summarized all of the coefficients for the main components of the excited states calculated by the SAC-CI, B3LYP and LC-BLYP. The calculated electronic structures of the excited states were more or less independent of the methods used. Among them, the LC-BLYP results were closer to the SAC-CI-NV results than to the B3LYP ones. In the first excited states of H_2PcCF_3, next HOMO to LUMO transition was a leading configuration in the SAC-CI-NV wave function, while HOMO to LUMO transition was a leading configuration in the B3LYP result. Introducing the long-range correction by the LC scheme, the coefficient for the HOMO → LUMO transition decreased, and the electronic structure became similar to those obtained by the SAC-CI-NV equations. These successful applications of the LC-BLYP functional indicate the applicability of the LC

Table 4 Calculated relative energy (kcal/mol) of configurational stereoisomers of H_2PcCF_3 compared with the total energy of the A-trans form

Computation[a]	A-trans	A-cis	B-trans	B-cis
B3LYP/Bas1	0.00	3.63	0.13	3.93
CAM-B3LYP/Bas3	0.00	2.77	0.10	2.99
MP2/Bas2	0.00	3.49	0.16	3.71

[a] Bas1: 6-31G*. Bas2: 6-31G** for H atoms at N atom of pyrrole rings and 6-31G* for the other atoms. Bas3: 6-311G**

scheme to the molecular design for the excited states of the porphycene compounds.

Before closing this section, we also examined a possibility of other configurational stereoisomers. Because of the observed X-ray structure [18], only the B-trans form was considered in the discussion above. Here, we evaluated the relative stability of the other isomers, A-trans, A-cis, and B-cis forms (for definition of the isomers, see Fig. 1b). In Table 4, relative energies of the isomers were compared. The energies of the cis isomers were about 3 kcal/mol higher than those of the trans isomers. It is interesting that the energy of the A-trans form is by 0.1 kcal/mol lower than that of the B-trans isomer in the B3LYP, CAM-B3LYP, and MP2 results. As shown in Figure S3 in supplementary material, structural parameters of the A-trans form are very similar to those of the B-trans form. The rms/maximum deviations in the bond lengths and bond angles calculated at the B3LYP/6-31G* level were 0.005/0.020 Å and 0.51°/0.91°, respectively. The deviation became larger in the dihedral angles: 5.07°/8.02°. The trend of the diagram seen in Figure S3 is similar to each other. The first excitation energy of the A-trans form calculated at the B3LYP/6-311G** and LC-BLYP/6-311G** levels was 2.06 and 1.65 eV, respectively, which were also close to those in the B-trans form (2.04 and 1.77 eV, respectively).

4 Conclusions

Quantum chemical calculations were performed to analyze the absorption spectrum and the redox potential of a recently synthesised fluorine-containing porphycene, 2,7,12,17-tetraethyl-3,6,13,16-tetrakis(trifluoromethyl) porphycene ($H_2Pc(EtioCF_3)$), in which the CF_3 groups at the β positions introduce unusual distortion in the porphycene macrocycle [18]. A particularly large positive-side shift (+0.8 V) was found in the reduction potential measured by cyclic voltammetry, and a large red-shift (−0.2 eV) of the Q band was observed in the absorption spectrum [18].

We started checking the applicability of the DFT exchange–correlation functionals by comparing the structural parameters (bond lengths, bond angles, and dihedral angles) between the calculated and X-ray crystallographic structures. The deviations were small enough to apply these functionals to the structural optimization of the distorted porphycene. On the basis of the relative energy and the magnitude of the deviations, the B-trans2 form (see Fig. 1c) was the most possible protonation state of $H_2Pc(EtioCF_3)$ in the crystal.

We tried to reproduce the experimental reduction and oxidation potentials of $H_2Pc(EtioCF_3)$ using available quantum chemical calculation methods. The particularly large shift of the reduction potential originates from a specifically large stabilization of the LUMO level due to both structural distortion and electronic effects introduced by the CF_3 groups. In order to reproduce the experimentally observed potentials, the solvent effect plays a crucial role. Extended basis sets were also necessary to achieve semiquantitative agreement with the experimental data. For improving the accuracy of the quantum chemical calculation of the redox potential in a future study, the environmental effect is a key point because the effect shares an essential portion of the reduction and oxidation potentials. On the other hand, for a qualitative discussion on the relative shift in the potentials, a quick and still acceptable approach is a KT level estimation using the orbital energies at neutral geometry.

Regarding the significant red-shift in the Q band absorption, we analyzed the electronic structures of the excited states of a series of porphycene compounds. The major contribution was from the molecular distortion effect introduced by the steric repulsions between the CF_3 groups. The second contribution arose from the electronic effect of the CF_3 groups. Both two effects caused the specific stabilization of the LUMO level and are the origin of the red-shift of the Q band.

In this study, we also aimed for establishing a computational scheme to calculate the redox potentials and the excited states of porphyrin-related compounds. The results are useful not only to understand the excited states and redox potential but also to help the computation-based molecular design for the functional molecules.

Acknowledgments The authors thank to Dr. R. Fukuda at Institute of Molecular Science for his fruitful comments on the SAC-CI calculations. This study was supported by KAKENHI (No. 21685002) from the Japan Society for the Promotion of Science (JSPS). This study was also supported by the JST-CREST and by a Grant-in-Aid for Young Scientists from the ACCMS and IIMC, Kyoto University. A portion of the computations was conducted at the RCCS (Okazaki, Japan).

References

1. Kadish KM, Smith KM, Guilard R (eds) (2000) The porphyrin handbook, vol 8, 9. Academic Press, New York

2. Dolphin D, Traylor TG, Xie LY (1997) Polyhaloporphyrins: unusual ligands for metals and metal-catalyzed oxidations. Acc Chem Res 30:251–259
3. Kadish KM, Royal G, Caemelbecke EV, Gueletti L (2000) Metalloporphyrins in nonaqueous media: database of redox potentials. In: Kadish KM, Smith KM, Guilard R (eds) The porphyrin handbook, vol 9. Academic Press, San Diego
4. Smith KM (1975) In: Smith KM (ed) Porphyrins and metalloporphyrins. Elsevier, Amsterdam, pp 872–889
5. Homma M, Aoyagi K, Aoyama Y, Ogoshi H (1983) Electron deficient porphyrins. 1. Tetrakis(trifluoromethyl)porphyrin and its metal complexes. Tetrahedron Lett 24:4343–4346
6. Vogel E, Kocher M, Schmickler H, Lex J (1986) Porphycene—a novel porphin isomer. Angew Chem Int Ed Engl 25:257–259
7. Renner MW, Forman A, Wu W, Chang CK, Fajer J (1989) Electrochemical, theoretical, and ESR characterizations of porphycenes. The.pi. anion radical of nickel(II) porphycene. J Am Chem Soc 111:8618–8621
8. Gisselbrecht JP, Gross M, Koecher M, Lausmann M, Vogel E (1990) Redox properties of porphycenes and metalloporphycenes as compared with porphyrins. J Am Chem Soc 112:8618–8620
9. Linstead RP, Whalley M (1952) Conjugated macrocylces. Part XXII. Tetrazaporphin and its metallic derivatives. J Chem Soc 4839–4845
10. Toyota K, Hasegawa J, Nakatsuji H (1996) SAC-CI study of the excited states of free base tetrazaporphin. Chem Phys Lett 250:437–442
11. Hasegawa J, Kimura T, Nakatsuji H (2005) Aza-substitution effect on the Q-band excitations of free-base porphin, chlorin, and bacteriochlorin: SAC-CI theoretical study. J Porphyr Phthalocyanines 9:305–315
12. Kadish KM, Smith KM, Guilard R (eds) (2003) The porphyrin handbook II, vol 16. Academic Press, New York
13. Toyota K, Hasegawa J, Nakatsuji H (1997) Excited states of Free Base Phthalocyanine studied by the SAC-CI method. J Phys Chem A 101:446–451
14. Kadish KM, Smith KM, Guilard R (eds) (2003) The porphyrin handbook II, vol 13. Academic Press, New York
15. Hasegawa J, Ozeki Y, Ohkawa K, Hada M, Nakatsuji H (1998) Theoretical study of the excited states of chlorin, bacteriochlorin, pheophytin *a*, and chlorophyll *a* by the SAC/SAC-CI method. J Phys Chem B 102:1320–1326
16. Waluk J, Muller M, Swiderek P, Kocher M, Vogel E, Hohlneicher G, Michl J (1991) Electronic states of porphycenes. J Am Chem Soc 113:5511–5527
17. Hasegawa J, Takata K, Miyahara T, Neya S, Frisch MJ, Nakatsuji H (2005) Excited states of porphyrin isomers and porphycene derivatives: A SAC-CI study. J Phys Chem A 109:3187–3200
18. Hayashi T, Nakashima Y, Ito K, Ikegami T, Aritome I, Suzuki A, Hisaeda Y (2003) Synthesis, structure, and chemical property of the first fluorine-containing porphycene. Org Lett 5:2845–2848
19. Nakatsuji H, Hasegawa J, Hada M (1996) Excited and ionized states of free base porphin studied by the SAC-CI method. J Chem Phys 104:2321–2329
20. Tokita Y, Hasegawa J, Nakatsuji H (1998) SAC-CI study on the excited and ionized states of free-base porphin: rydberg excited states and effect of polarization and rydberg functions. J Phys Chem A 102:1843–1849
21. Hasegawa J, Hada M, Nonoguchi M, Nakatsuji H (1996) Ground and excited states of Mg porphin studied by the SAC/SAC-CI method. Chem Phys Lett 250:159–164
22. Nakatsuji H, Hirao K (1978) Cluster expansion of the wavefunction. Symmetry-adapted-cluster (SAC) expansion, its variational determination, and extension of open-shell orbital theory. J Chem Phys 68:2053–2065
23. Nakatsuji H (1978) Cluster expansion of the wavefunction. Excited states. Chem Phys Lett 59:362–364
24. Nakatsuji H (1979) Cluster expansion of the wavefunction. Electron correlations in ground and excited states by SAC (Symmetry-Adapted-Cluster) and SAC-CI theories. Chem Phys Lett 67(2,3):329–333
25. Nakatsuji H (1979) Cluster expansion of the wavefunction. Calculation of electron correlations in ground and excited states by SAC and SAC-CI theories. Chem Phys Lett 67(2,3):334–342
26. Nakatsuji H (1992) Electronic structures of ground, excited, ionized, and anion states studied by the SAC/SAC-CI theory. Acta Chim Hung 129:719–776
27. Nakatsuji H (1997) SAC-CI method: theoretical aspects and some recent topics. In: Leszczynski J (ed) Computational chemistry–reviews of current trends, vol. 2, vol 2. World Scientific, Singapore, pp 62–124
28. Fukuda R, Nakatsuji H (2008) Formulation and implementation of direct algorithm for the symmetryadapted cluster and symmetry-adapted cluster–configuration interaction method. J Chem Phys 128:094105
29. Frisch MJ, Trucks GW, Schlegel HB, Scuseria GE, Robb MA, Cheeseman JR, Scalmani G, Barone V, Mennucci B, Petersson GA, Nakatsuji H, Caricato M, Li X, Hratchian HP, Izmaylov AF, Bloino J, Zheng G, Sonnenberg JL, Hada M, Ehara M, Toyota K, Fukuda R, Hasegawa J, Ishida M, Nakajima T, Honda Y, Kitao O, Nakai H, Vreven T, Montgomery JA Jr, Peralta JE, Ogliaro F, Bearpark M, Heyd JJ, Brothers E, Kudin KN, Staroverov VN, Keith T, Kobayashi R, Normand J, Raghavachari K, Rendell A, Burant JC, Iyengar SS, Tomasi J, Cossi M, Rega N, Millam JM, Klene M, Knox JE, Cross JB, Bakken V, Adamo C, Jaramillo J, Gomperts R, Stratmann RE, Yazyev O, Austin AJ, Cammi R, Pomelli C, Ochterski JW, Martin RL, Morokuma K, Zakrzewski VG, Voth GA, Salvador P, Dannenberg JJ, Dapprich S, Daniels AD, Farkas O, Foresman JB, Ortiz JV, Cioslowski J, Fox DJ (2010) Gaussian 09, revision B.01. Gaussian, Inc., Pittsburgh
30. Hehre WJ, Ditchfield R, Pople JA (1972) Self-consistent molecular orbital methods. XII. Further extensions of gaussian-type basis sets for use in molecular orbital studies of organic molecules. J Chem Phys 56:2257–2261
31. Hariharan PC, Pople JA (1973) The influence of polarization functions on molecular orbital hydrogenation energies. Theor Chim Acta 28:213–222
32. Krishnan R, Binkley JS, Seeger R, Pople JA (1980) Self-consistent molecular orbital methods. XX. A basis set for correlated wave functions. J Chem Phys 72:650–654
33. Becke AD (1993) Density-functional thermochemistry. III. The role of exact exchange. J Chem Phys 98:5648–5652
34. Lee C, Yang W, Parr RG (1988) Development of the Colle-Salvetti correlation-energy formula into a functional of the electron density. Phys Rev B 37:785–789
35. Kristyán S, Pulay P (1994) Can (semi)local density functional theory account for the London dispersion forces? Chem Phys Lett 229:175–180
36. Kannemann FO, Becke AD (2010) van der Waals interactions in density-functional theory: intermolecular complexes. J Chem Theory Comput 6:1081–1088
37. Mackie ID, DiLabio GA (2008) Interactions in large, polyaromatic hydrocarbon dimers: application of density functional theory with dispersion corrections. J Phys Chem A 112:10968–10976
38. Yanai T, Tew DP, Handy NC (2004) A new hybrid exchange-correlation functional using the Coulomb-Attenuating Method (CAM-B3LYP). Chem Phys Lett 393:51–57
39. Chai J-D, Head-Gordon M (2008) Long-range corrected hybrid density functionals with damped atom-atom dispersion corrections. Phys Chem Chem Phys 10:6615–6620

40. Cancès MT, Mennucci B, Tomasi J (1997) A new integral equation formalism for the polarizable continuum model: theoretical background and applications to isotropic and anisotropic dielectrics. J Chem Phys 107:3032–3041
41. Baik M-H, Friesner RA (2002) Computing redox potentials in solution: density functional theory as a tool for rational design of redox agent. J Phys Chem A 106:7407–7412
42. Fu Y, Liu L, Yu H-Z, Wang Y-M, Guo Q-X (2005) Quantum-chemical predictions of absolute standard redox potentials of diverse molecules and free radicals in acetonitrile. J Am Chem Soc 127:7227–7234
43. Atkins PW (1998) Physical chemistry. Oxford University Press, Oxford
44. Trasatti S (1986) The absolute electrode potential: an explanatory note. Pure Appl Chem 58:955–966
45. Casida ME (1996) Time-dependent density functional response theory of molecular systems: theory, computational methods, and functionals. In: Seminario JM (ed) Recent developments and applications of modern density functional theory. Elsevier Science, Amsterdam
46. Bauernschmitt R, Ahlrichs R (1996) Treatment of electronic excitations within the adiabatic approximation of time dependent density functional theory. Chem Phys Lett 156:454–464
47. Iikura H, Tsuneda T, Yanai T, Hirao K (2001) Long-range correction scheme for generalized-gradient-approximation exchange functionals. J Chem Phys 115:3540–3544
48. Becke AD (1997) Density-functional thermochemistry. V. systematic optimization of exchange-correlation functionals. J Chem Phys 107:8554–8560
49. Dunning Jr TH, Hay PJ (1976) Gaussian basis sets for molecular calculations. In: Schaefer III HF (ed) Modern theoretical chemistry, vol 3. Plenum, New York, pp 1–28
50. Gouterman M (1961) Spectra of porphyrins. J Mol Spectrosc 6:138–163
51. Yamaguchi K, Takahara Y, Fueno T, Houk KN (1988) Extended Hartree-Fock (EHF) theory of chemical reactions. Theo Chem Acc 73:337–364
52. Yamanaka S, Okumura M, Nakano M, Yamaguchi K (1994) EHF theory of chemical reactions Part 4. UNO CASSCF, UNO CASPT2 and R(U)HF coupled-cluster (CC) wavefunctions. J Mol Struct 310:205–218
53. Tawada Y, Tsuneda T, Yanagisawa S, Yanai T, Hirao K (2004) A long-range-corrected time-dependent density functional theory. J Chem Phys 120:8425–8433